DØNote 5056-CONF

Limits on Standard Model Higgs Boson Production

The DØ Collaboration
(Dated: March 20, 2006)

Upper limits on the cross section for Standard Model Higgs boson production in $p\bar{p} \to H + X$ at $\sqrt{s} = 1.96$ TeV are determined for $100 < m_H < 200$ GeV/c^2. The contributing processes include associated production ($WH \to e\nu b\bar{b}$, $WH \to \mu\nu b\bar{b}$, $ZH \to \nu\nu b\bar{b}$, and $WH \to WW^+W^-$) and gluon fusion ($H \to W^+W^-$). Analyses are conducted with integrated luminosities from 261 pb^{-1}to 385 pb^{-1}. Limits for various combinations of the channels are presented. The final combination is also presented including the most recent DØ result obtained in the $H \to W^+W^-$ channel with 950 pb^{-1}of data. The 95% CL upper limits are a factor of 15(7) away from the Standard Model cross section at m_H =115(160) GeV/c^2.

Preliminary Results for Winter 2006 Conferences

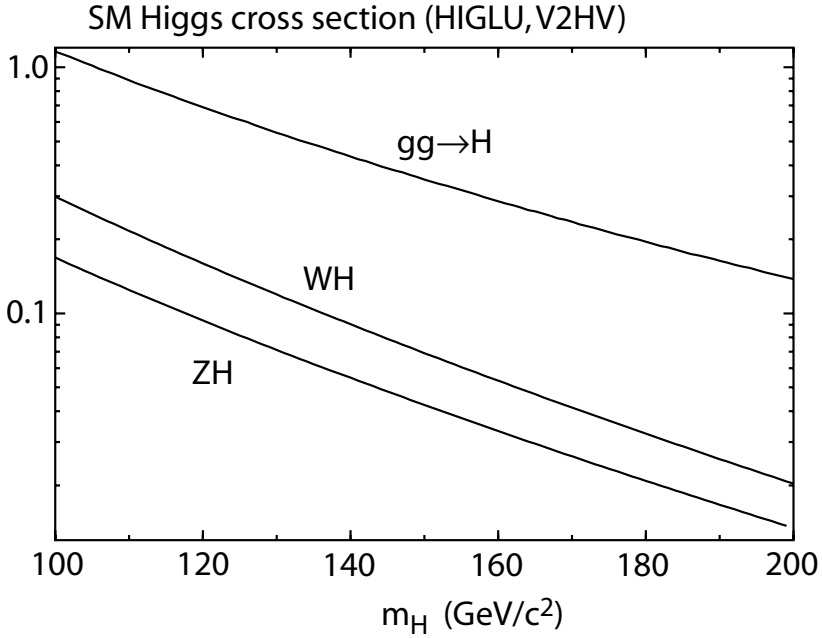

FIG. 1: Production cross sections for a SM Higgs boson in $p\bar{p}$ collisions at $\sqrt{s} = 1.96$ TeV as a function of Higgs mass[3].

I. INTRODUCTION

Despite its success as a predictive tool, the Standard Model (SM) of particle physics remains incomplete without a means to explain gauge-symmetry breaking. The simplest proposed mechanism involves the introduction of a complex doublet of scalar fields that generate particle masses via their mutual interactions. This so-called Higgs mechanism also introduces a single scalar boson with an unpredicted mass. Direct searches in $e^+e^- \to Z^* \to ZH$ at the Large Electron Positron (LEP) collider yielded lower mass limits at $m_H > 114.4$ GeV/c^2[1] and the SM Higgs boson search is ongoing at the Fermilab Tevatron collider.

In this note, we present and combine results on direct searches for SM Higgs bosons in $p\bar{p}$ collisions at $\sqrt{s} = 1.96$ TeV recently presented by DØ [2]. These are searches for Higgs bosons produced in association with vector bosons ($p\bar{p} \to WH/ZH \to \ell\nu b\bar{b}, \nu\nu b\bar{b}$, $p\bar{p} \to WH \to WW^+W^-$) or produced via gluon-gluon fusion ($p\bar{p} \to H \to W^+W^-$). The production cross sections and branching fractions for these decays are shown in Figs 1 and 2 respectively.

The searches were conducted with data collected during the period 2003-2005 and correspond to integrated luminosities ranging from 261 pb^{-1}to 385 pb^{-1}and separated into fourteen orthogonal final states, referred to as analyses in the following. Each analysis is designed to maximize the search sensitivity for a particular single final state defined by a Higgs boson production and decay mode. In order to ensure proper combination of signals, the analyses were designed to be mutually exclusive after analysis selections. In addition, the final combination is presented including the most recent DØ result obtained in the $H \to W^+W^-$ channel with 950 pb^{-1}of data. The Higgs signals were generated by `PYTHIA` v6.202[5] using `CTEQ5L`[6] leading order parton distribution functions. The signal cross sections and branching ratios were calculated using `HIGLU`[3], `V2HV`[3], and `HDECAY`[4]. Backgrounds were generated by `PYTHIA`, `ALPGEN`[7], and `COMPHEP`[8], with `PYTHIA` providing parton-showering and hadronization for all. Background cross sections were normalized to next-to-leading order calculations from `MCFM`[9] in all possible cases.

II. LIMIT CALCULATIONS

We combine results using the CL_s method with a log-likelihood ratio (LLR) test statistic[10]. This method provides a robust means of combining individual channels while incorporating systematic uncertainties. Systematics are treated as uncertainties on the expected numbers of signal and background events, not the outcome of the limit calculation. This approach ensures that the uncertainties and their correlations are propagated to the outcome with their proper weights. The CL_s approach used here utilizes binned final-variable distributions rather than a single-bin (fully integrated) value.

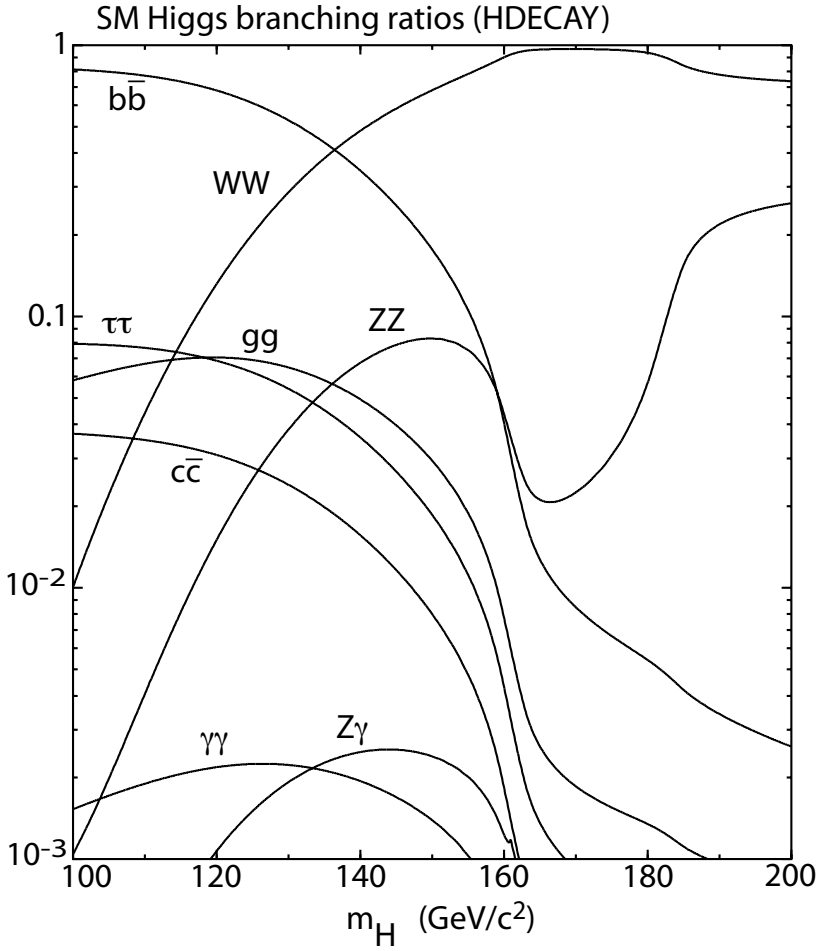

FIG. 2: Branching fractions for a SM Higgs boson. These values were calculated using the HDECAY program[4].

A. Final Variable Preparation

In the case of the $H \to b\bar{b}$ analyses, the final variable used for limit setting is the invariant dijet mass, either when requiring one jet being tagged as a b-jet, or when the two jets used for the dijet mass are both tagged as b-jets. Examples of these two types of distribution are given in Figs. 3a,b. In the $H \to W^+W^-$ analyses, the Higgs mass cannot be directly reconstructed due to the neutrinos in the final state. Thus, the $WH \to WW^+W^-$ analysis uses a likelihood discriminant as final variable, as shown in Fig. 3c, and the $H \to W^+W^-$ analysis uses the difference in φ between the two final state leptons, shown in Fig. 3d.

Each signal and background final variable distribution is smoothed via Gaussian kernel estimation[12]. In a few instances, the statistics of a Monte Carlo-derived background source are too small to properly describe the expected shape of the final-variable distribution. In these cases, the shape is taken from a higher statistics sample of the same background and the proper normalization is applied. For example, after applying a double b-tag selection in the $WH \to \mu\nu b\bar{b}$ analysis, the dijet mass final variable for the the $W + 2$ jet background retains only four events. The resulting dijet mass distribution is too small to reliably estimate this background shape. To partially correct for this effect, the background shape is taken from the $W+2$ jet single-tag selection with the double-tag normalization applied. In this manner, the systematic uncertainty associated with the shape of the final variable is greatly reduced [11].

To decrease the granularity of the steps between simulated Higgs masses in the limit calculation, additional Higgs mass points are created via signal point interpolation[12]. The primary motivation of this procedure is to provide a means for combining analyses which do not share a common simulated Higgs mass. However, this procedure also provides a measurement of the behavior of each limit on a finer granularity than otherwise possible.

Source	$WH \to e\nu b\bar{b}$	$WH \to \mu\nu b\bar{b}$	$WH \to \ell\nu b\bar{b}$	$ZH \to \nu\nu b\bar{b}$	$WH \to WW^+W^-$	$H \to W^+W^-$
Luminosity	×	×	×	×	×	×
Jet Energy Scale	×	×	×	×		×
Jet ID	×	×	×	×		
Electron ID	×				×	×
Muon ID		×			×	×
b-Jet Tagging	×	×	×	×		
Background σ	×	×	×	×	×	×

TABLE I: List of leading correlated systematic uncertainties and the analyses in which they apply. The correlated systematic uncertainty on the background cross section (σ) is itself subdivided according to the different backgrounds processes used in each analysis.

B. Systematic Uncertainties

The systematic uncertainties differ between analyses for both the signals and backgrounds[13–17]. Here we will summarize only the largest contributions. All analyses carry an uncertainty on the luminosity of 6.5%. The $H \to b\bar{b}$ analyses have an uncertainty on the b-tagging rate of 4-6% per tagged jet (tag normalization and taggability). These analyses also have an uncertainty on the jet measurement and acceptances of $\sim 7.5\%$ (jet-ID, JES, and jet smearing). For the $H \to W^+W^-$ decays, the largest uncertainties are associated with lepton measurement and acceptances. These values range from 3-6% depending on the final state. The largest contributing factors for all analyses is the uncertainty on the background cross sections at 5-18%.

The systematic uncertainties for the background rate are generally several times larger than the signal expectation and are thus an important factor in the calculation of limits. As such, each systematic uncertainty is folded into the signal and background expectations via Gaussian distribution according to its size. The Gaussian values are sampled once for each Poisson MC trial (pseudo-experiment). Correlations between systematic sources are carried through in the calculation. For example, the uncertainty on the luminosity is held to be correlated between all signals and backgrounds and, thus, the same fluctuation in the luminosity is common to all channels. All systematic uncertainties originating from a common source are held to be correlated, as detailed in Table I.

III. DERIVED LIMITS

We derive limits on SM Higgs boson production $\sigma \times BR(H \to X)$ via fourteen individual analyses[13–17]. These analyses are categorized by their production processes and outlined in Table II along with their corresponding integrated luminosities. In the cases of $p\bar{p} \to W/ZH$ production, we search for both $H \to b\bar{b}$ and $H \to W^+W^-$ decays. For $H \to b\bar{b}$ decays, the analyses are separated into two orthogonal groups: one group in which two of the b-quarks were tagged via b-jet identification or b-tagging (double-tag or DT) and one group in which only one b-quark was tagged (single-tag or ST). The decays of the vector bosons further define the analyzed final states: $WH \to e\nu b\bar{b}$, $WH \to \mu\nu b\bar{b}$, and $ZH \to \nu\nu b\bar{b}$. There is a sizable amount of $WH \to \ell\nu b\bar{b}$ signal that can mimic the $ZH \to \nu\nu b\bar{b}$ final state when the lepton is undetected. This case is treated as a separate WH analysis, to which we refer as $WH \to \ell\nu b\bar{b}$. We also include an analysis of $WH \to WW^+W^-$ final states. Here the associated W boson and the same-charged W boson from the Higgs decay are required to decay semi-leptonically, thus defining six final states: $WH \to We^{\pm}\nu e^{\pm}\nu$, $WH \to We^{\pm}\nu\mu^{\pm}\nu$, and $WH \to W\mu^{\pm}\nu\mu^{\pm}\nu$. All decays of the third W boson are included. In the case of $p\bar{p} \to H \to W^+W^-$ production, we again search for semi-leptonic W boson decays with four final states: $WW \to e^+\nu e^-\nu$, $WW \to e^{\pm}\nu\mu^{\mp}\nu$, and $WW \to \mu^+\nu\mu^-\nu$. For the gluon fusion process, $H \to b\bar{b}$ decays are not considered due to the large multijets background.

A. Results for Individual Channels

Figure 4 shows the log-likelihood ratio (LLR) distributions for $WH(H \to b\bar{b}$, ST+DT), $ZH \to \nu\nu b\bar{b}$ (ST+DT), $WH \to WW^+W^-$, and $H \to W^+W^-$ final states, respectively. Included in these figures are the LLR values for the signal+background hypothesis (LLR_{s+b}), background-only hypothesis (LLR_b), and the observed data (LLR_{obs}). The shaded bands represent the 1-σ and 2-σ regions for the background-only hypothesis. Frequently, the LLR value is also denoted as $-2\ln Q$ and can be interpreted as follows:

Channel	Luminosity (pb^{-1})	Final Variable	Reference
$WH \to e\nu bb$ ST	371	Dijet mass	[13]
$WH \to e\nu b\bar{b}$ DT	371	Dijet mass	[13]
$WH \to \mu\nu b\bar{b}$ ST	385	Dijet mass	[14]
$WH \to \mu\nu b\bar{b}$ DT	385	Dijet mass	[14]
$WH \to WW^+W^-$ ($e^\pm e^\pm$)	384	Likelihood discriminant	[15]
$WH \to WW^+W^-$ ($e^\pm \mu^\pm$)	368	Likelihood discriminant	[15]
$WH \to WW^+W^-$ ($\mu^\pm \mu^\pm$)	363	Likelihood discriminant	[15]
$WH \to \ell\nu b\bar{b}$ ST	261	Dijet mass	[16]
$WH \to \ell\nu b\bar{b}$ DT	261	Dijet mass	[16]
$ZH \to \nu\nu b\bar{b}$ ST	261	Dijet mass	[16]
$ZH \to \nu\nu b\bar{b}$ DT	261	Dijet mass	[16]
$H \to W^+W^- \to e^\pm \nu e^\mp \nu$	325	$\Delta\varphi(e^\pm, e^\mp)$	[17]
$H \to W^+W^- \to e^\pm \nu \mu^\mp \nu$	318	$\Delta\varphi(e^\pm, \mu^\mp)$	[17]
$H \to W^+W^- \to \mu^\pm \nu \mu^\mp \nu$	299	$\Delta\varphi(\mu^\pm, \mu^\mp)$	[17]

TABLE II: List of analysis channels, corresponding integrated luminosities, and final variables.

- The separation between LLR_b and LLR_{s+b} provides a measure of the overall search power of the analysis. This is the ability of the analysis to separate the $s+b$ and $b-$only hypotheses.
- The width of the LLR_b distribution gives an estimate of how sensitive the analysis is to a signal-like fluctuation. For example, when a 1-σ background fluctuation is large compared to the signal expectation, the analysis sensitivity is limited.
- The value of the LLR_{obs} indicates whether the data distribution appears to be more signal-like or background-like, depending on where the observed value falls with respect to the LLR_b and LLR_{s+b} values. Furthermore, the width of the LLR_b distribution gives a measure of the significance of any departures from the $b-$only expectation.

B. Combined Results

The individual analyses described above can be grouped to form several combined limits. Here we present the following limits:

- All WH searches (ST,DT, and $WH \to WW^+W^-$) in the low-mass range ($m_H = 100 - 145$ GeV/c^2).
- All ZH searches (ST and DT) in the low-mass range ($m_H = 100 - 145$ GeV/c^2).
- All WH, ZH, and $H \to W^+W^-$ searches over the full mass range ($m_H = 100 - 200$ GeV/c^2).

Figure 5 shows the expected and observed 95% CL cross section limits for the combined WH analyses ($WH \to e, \mu,$ / $\ell\nu b\bar{b}$ (ST and DT), and $WH \to WW^+W^-$). These limits are given with respect to the sum of $\sigma(p\bar{p} \to WH) \times BR(H \to b\bar{b})$ and $\sigma(p\bar{p} \to WH) \times BR(H \to W^+W^-)$ at $\sqrt{s} = 1.96$ TeV.

Figure 6 shows the expected and observed 95% CL cross section limits for the combined $ZH \to \nu\nu b\bar{b}$ analyses (ST and DT). These limits are given with respect to $\sigma(p\bar{p} \to ZH) \times BR(H \to b\bar{b})$ at $\sqrt{s} = 1.96$ TeV.

Figure 7 shows the expected and observed 95% CL cross section limits for all analyses combined in the low-mass region ($m_H = 100 - 145$ GeV/c^2). These limits are given with respect to the sum of $\sigma(p\bar{p} \to WH/ZH) \times BR(H \to b\bar{b})$, $\sigma(p\bar{p} \to WH) \times BR(H \to W^+W^-)$, and $\sigma(p\bar{p} \to H) \times BR(H \to W^+W^-)$ at $\sqrt{s} = 1.96$ TeV. Figure 8 shows the ratio of each limit to the SM cross section. Figures 9 and 10 give these same distributions for the full mass region ($m_H = 100 - 200$ GeV/c^2).

Compared to earlier studies on simulation that also covered the full mass range[18], our results, which use more channels and study them on a wider mass range, show that the region between $m_H = 115 - 190$ GeV/c^2 is probed more uniformly than predicted. Indeed there is only a factor of 2 difference in sensitivity between the most and the least sensitive region in this mass range.

IV. CONCLUSIONS

We have presented results for fourteen Higgs search analyses. We have combined these analyses to form new limits more sensitive than each individual limit.

- Combined limits on $\sigma(p\bar{p} \to WH) \times BR(H \to b\bar{b}/W^+W^-)$ range from 2.8 pb at $m_H = 115$ GeV/c^2 to 3.1 pb at $m_H = 145$ GeV/c^2 (3.5 pb to 2.6 pb expected limits).
- Combined limits on $\sigma(p\bar{p} \to ZH) \times BR(H \to b\bar{b})$ range from 3.1 pb at $m_H = 115$ GeV/c^2 to 2.2 pb at $m_H = 145$ GeV/c^2 (2.8 pb to 2.0 pb expected limits).
- Fully combined limits on Higgs production ($\sigma(p\bar{p} \to WH/ZH/H) \times BR(H \to b\bar{b}/W^+W^-)$) range from 4.3 pb at $m_H = 115$ GeV/c^2, 6.4 pb at $m_H = 135$ GeV/c^2, 4.2 at $m_H = 160$, and 4.3 pb at $m_H = 190$ GeV/c^2 (4.8 pb, 6.8 pb, 3.8, and 4.1 expected limits), with corresponding ratios to the SM cross section of 15, 22, 13, and 28 (16, 23, 12, and 29 expected ratios).

These relatively high cross section ratios will decrease strongly in the near future with the luminosity recorded at the Tevatron: more than 1 fb^{-1}is currently being analyzed and 8 fb^{-1}are expected by the end of 2009. To illustrate the impact of larger luminosity, we have performed the full combination with a preliminary result for two $H \to W^+W^-$ channels ($e^{\pm}\nu e^{\mp}\nu$ and $e^{\pm}\nu\mu^{\mp}\nu$) at 950 pb^{-1}[19]. In Fig. 11 we compare the combined expected limit obtained with the 261-385 pb^{-1} $H \to W^+W^-$ analyses to the new combined expected limit derived by replacing the low statistics ($e^{\pm}\nu e^{\mp}\nu$ and $e^{\pm}\nu\mu^{\mp}\nu$) channels with the high statistics (950 pb^{-1}) ones. Both combinations use the same low luminosity $\mu^{\pm}\nu\mu^{\mp}\nu$ channel. As expected, the improvement is visible for $m_H >$125 GeV/c^2. In Fig. 12 the new observed limit is compared to the 261-385 pb^{-1}combined limits. For $m_H =$160 GeV/c^2, the new observed limit is less than a factor 7 away from the SM expectation.

Furthermore we are developing new techniques to improve the current sensitivity: we expect improvements via multivariate analyses ($\sim$ 70% increase in sensitivity), neural-network b-tagging ($\sim$ 35%), and improved dijet mass resolution ($\sim$ 20%). These improvements will occur simultaneously with the introduction of additional search channels that will add $\sim$ 15% in sensitivity. In addition, an anticipated combination with the results from the CDF experiment would yield an increase in sensitivity of $\sim$ 40%. As such, we are optimistic about the near-future prospects of the SM Higgs search at the Tevatron.

Acknowledgments

We thank the staffs at Fermilab and collaborating institutions, and acknowledge support from the DOE and NSF (USA); CEA and CNRS/IN2P3 (France); FASI, Rosatom and RFBR (Russia); CAPES, CNPq, FAPERJ, FAPESP and FUNDUNESP (Brazil); DAE and DST (India); Colciencias (Colombia); CONACyT (Mexico); KRF and KOSEF (Korea); CONICET and UBACyT (Argentina); FOM (The Netherlands); PPARC (United Kingdom); MSMT (Czech Republic); CRC Program, CFI, NSERC and WestGrid Project (Canada); BMBF and DFG (Germany); SFI (Ireland); Research Corporation, Alexander von Humboldt Foundation, and the Marie Curie Program.

[1] Phys.Lett. B565 (2003) 61-75
[2] DØ Collaboration, V. Abazov *et al.*, "The Upgraded D0 Detector", submitted to Nucl. Instrum. Methods Phys. Res. A
[3] Phys. Lett. B273 (1991) 167
[4] A. Djouadi, J. Kalinowski, M. Spira, Comp. Phys. Commun. 108 C (1998) 56
[5] T. Sjöstrand *et al.*, PYTHIA *6.2: PHYSICS AND MANUAL,* e-Print Archive: hep-ph/0108264, LU-TP-01-21, Lund 2001
[6] H. L. Lai *et al.*, *Improved Parton Distributions from Global Analysis of Recent Deep Inelastic Scattering and Inclusive Jet Data,* Phys. Rev. **D**55 (1997) 1280
[7] M. Mangano et al.: ALPGEN, a generator for hard multiparton processes in hadron collisions, hep-ph/0206293
[8] A. Pukhov *et al.*, COMPHEP , hep-ph/9908288 (1999)
[9] J. Campbell and K. Ellis, MCFM, Montecarlo for FeMtobarn processes, http://mcfm.fnal.gov/
[10] T. Junk, Nucl.Instrum.Meth.A434, p. 435-443, 1999
[11] The procedure of replacing very low statistics MC samples with a higher statistics version was performed for the following background/analysis combinations: $W/Z + 2$jet ($WH \to e, \mu\nu b\bar{b}$); $Z \to e^+e^-, \tau^+\tau^-$ ($H \to e^+\nu e^-\nu$).
[12] W. Fisher, DØ Note #4975
[13] $WH \to e\nu b\bar{b}$ analysis, DØ Conference Note 5054

[14] $WH \to \mu\nu b\bar{b}$ analysis, DØ Conference Note 5054
[15] $WH \to WW^+W^-$ analysis, DØ Note 5021
[16] $ZH \to \nu\nu b\bar{b}$ analysis note, DØ Conference Note 5060
[17] DØ Collaboration, Phys. Rev. Lett. 96, 011801 (2006)
[18] M. Carena, J. Conway, H. Haber, J. Hobbs et al., FERMILAB-CONF-00/279-T (2000), hep-ph/0010338
[19] DØ Conference Note 5063

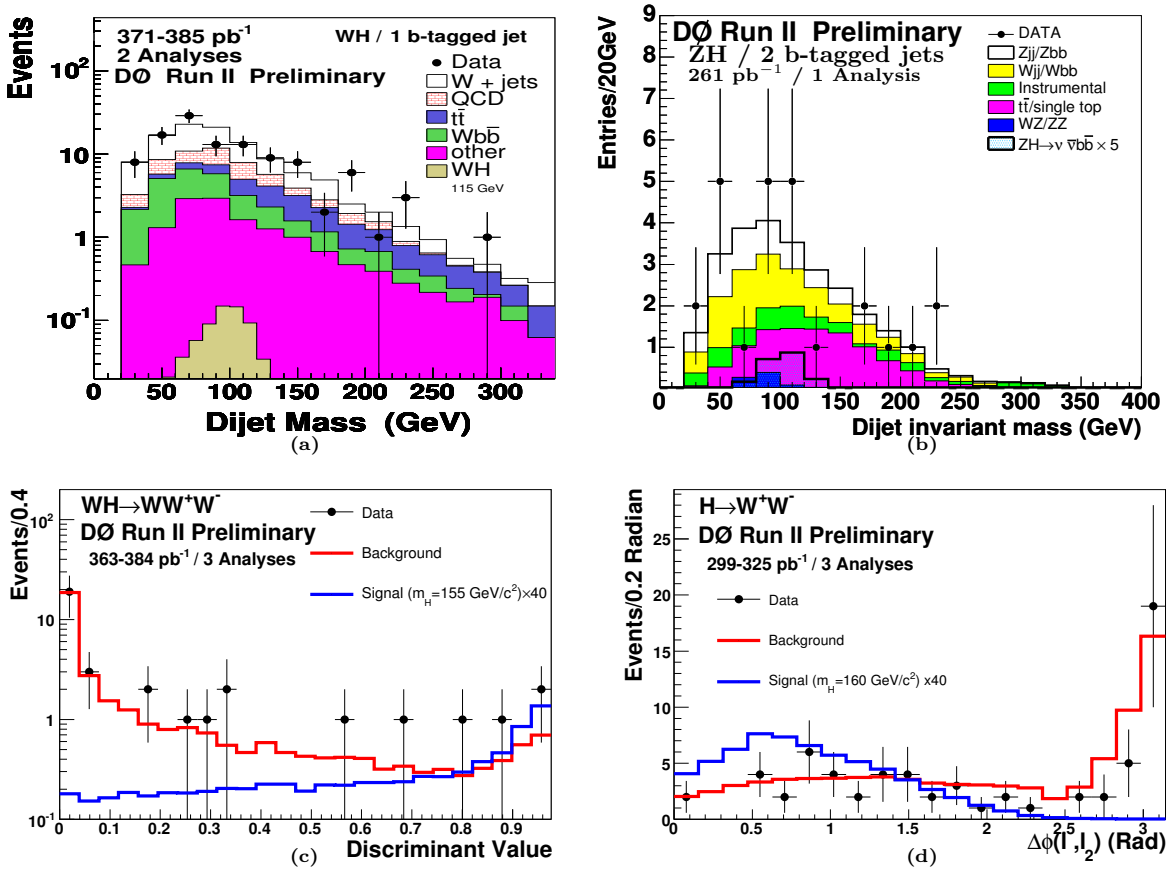

FIG. 3: Final variable distributions for selected Higgs search analyses. Shown in the figure are the distributions for: the invariant mass for $WH \to e, \mu\nu b\bar{b}$ ST analyses (a), the invariant mass for the $ZH \to \nu\nu b\bar{b}$ DT analysis (b), the likelihood discriminant for the $WH \to WW^+W^-$ analyses (c), and $\Delta\varphi(\ell_1, \ell_2)$ for the $H \to W^+W^-$ analyses (d). For all figures, background expectations and observed data are shown. Also shown are selected Higgs mass signals with indicated scaling factors.

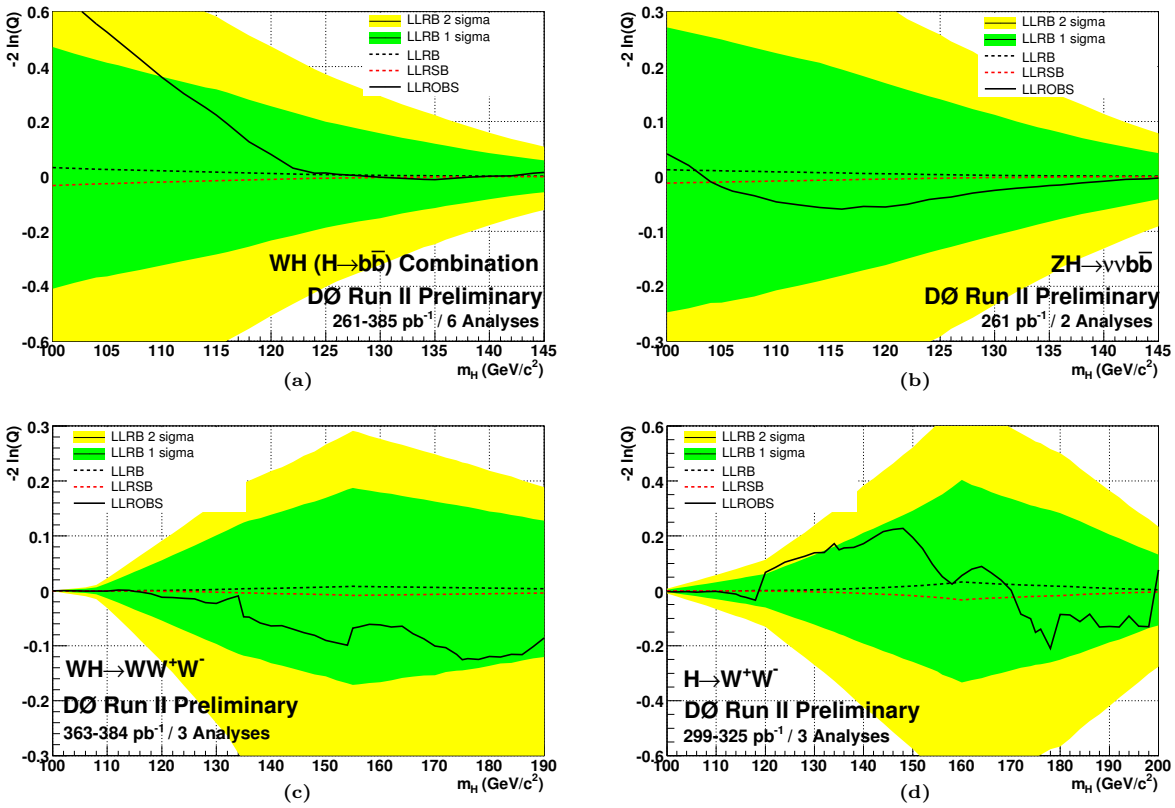

FIG. 4: Log-likelihood ratio distribution for the WH ($H \to b\bar{b}$) analyses ($WH \to e, \mu$, $\not\ell\nu b\bar{b}$, ST+DT final states combined) (a), the $ZH \to \nu\nu b\bar{b}$ ST+DT combined channels (b), the $WH \to WW^+W^-$ channels (c), and the $H \to W^+W^-$ analyses (e^+e^-, $e\mu$, and $\mu^+\mu^-$ final states combined) (d). Shown in the plot are the LLR_b (background-only hypothesis), LLR_{s+b} (signal+background hypothesis), LLR_{obs} (observed LLR value), and the 1-σ and 2-σ bands for the LLR_b distribution.

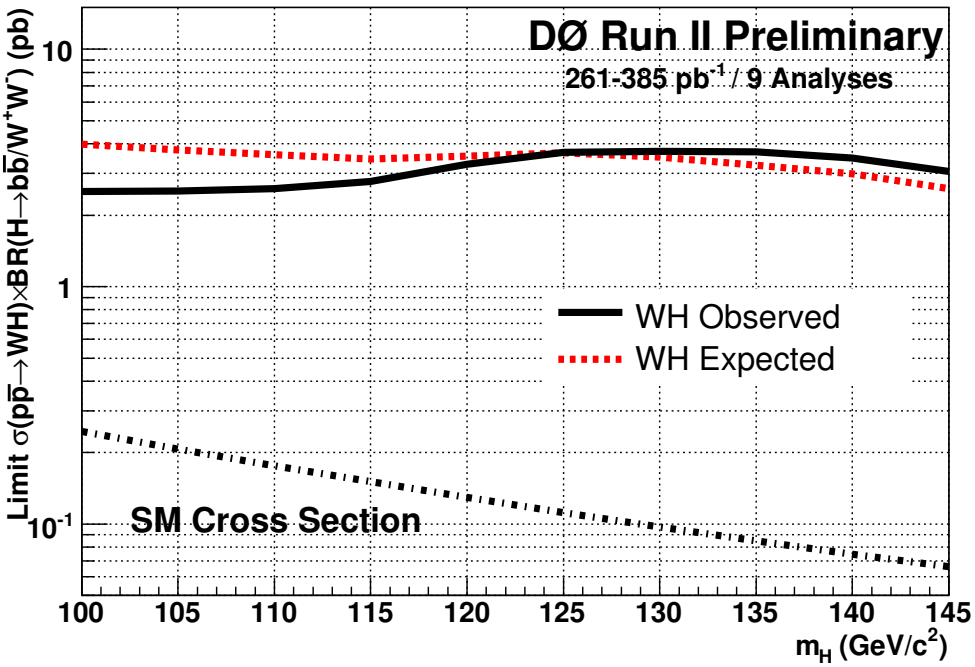

FIG. 5: Expected (median) and observed 95% CL limits for the WH analyses ($WH \to e, \mu$, $\not\!\!\nu b\bar{b}$ and $WH \to WW^+W^-$ final states combined). These limits are given with respect to the sum of $\sigma(p\bar{p} \to WH) \times BR(H \to b\bar{b})$ and $\sigma(p\bar{p} \to WH) \times BR(H \to W^+W^-)$ at $\sqrt{s} = 1.96$ TeV.

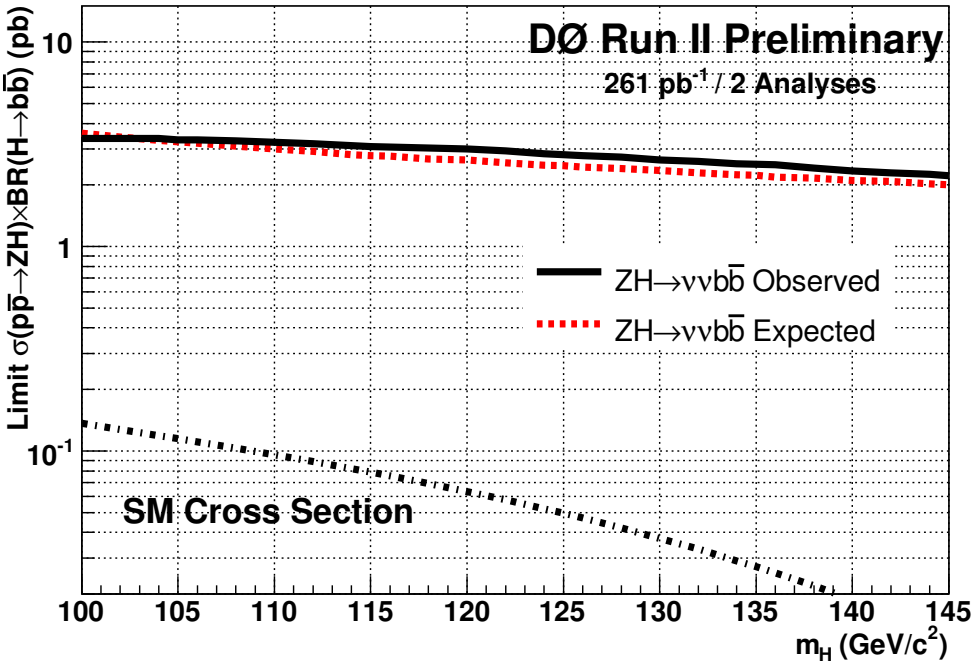

FIG. 6: Expected (median) and observed 95% CL limits for the $ZH \to \nu\nu b\bar{b}$ combined ST and DT analyses. These limits are given with respect to $\sigma(p\bar{p} \to ZH) \times BR(H \to b\bar{b})$ at $\sqrt{s} = 1.96$ TeV.

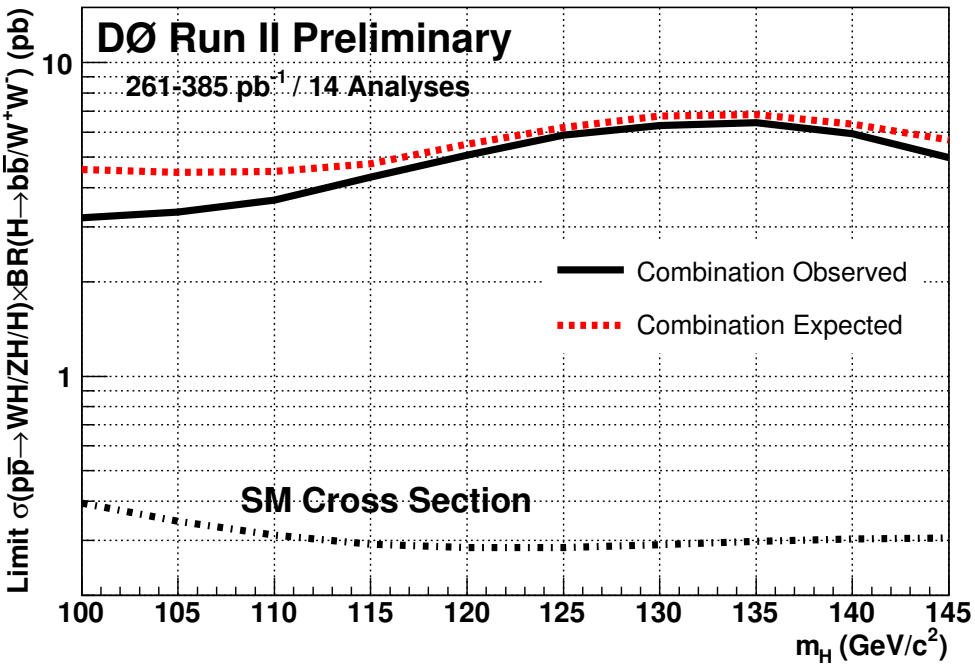

FIG. 7: Expected (median) and observed 95% CL limits for the $WH/ZH/H$ analyses ($WH \to e,\mu$, $\not\ell\nu b\bar{b}$, $ZH \to \nu\nu b\bar{b}$, $WH \to WW^+W^-$, and $H \to W^+W^-$ final states combined). These limits are given with respect to the sum of $\sigma(p\bar{p} \to WH/ZH) \times BR(H \to b\bar{b})$, $\sigma(p\bar{p} \to WH) \times BR(H \to W^+W^-)$, and $\sigma(p\bar{p} \to H) \times BR(H \to W^+W^-)$ at $\sqrt{s} = 1.96$ TeV.

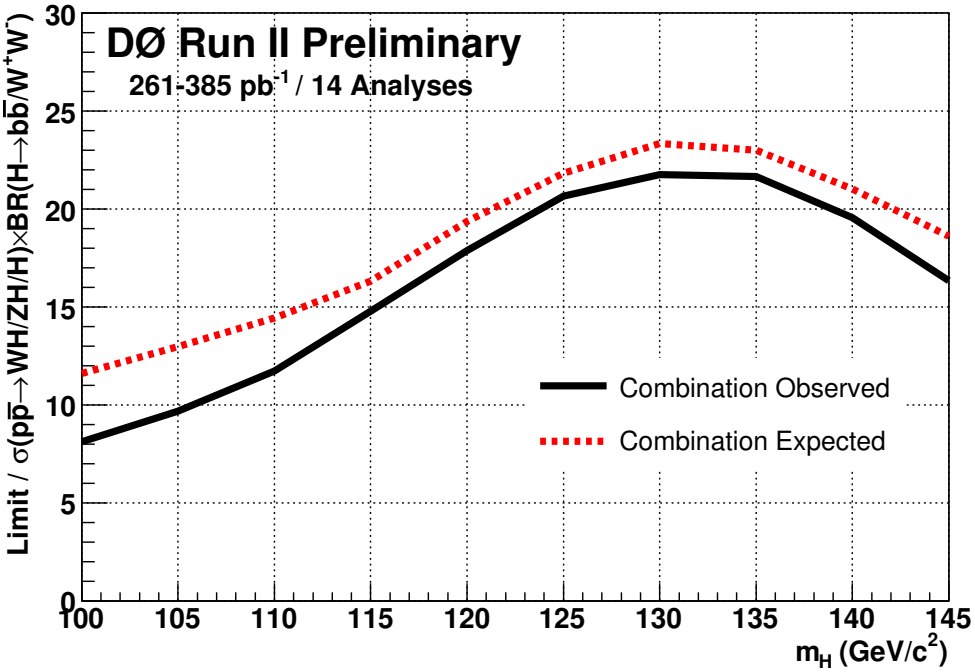

FIG. 8: Expected (median) and observed cross section ratios (95% CL limit to SM cross section) for the $WH/ZH/H$ analyses ($WH \to e,\mu$, $\not\ell\nu b\bar{b}$, $ZH \to \nu\nu b\bar{b}$, $WH \to WW^+W^-$, and $H \to W^+W^-$ final states combined).

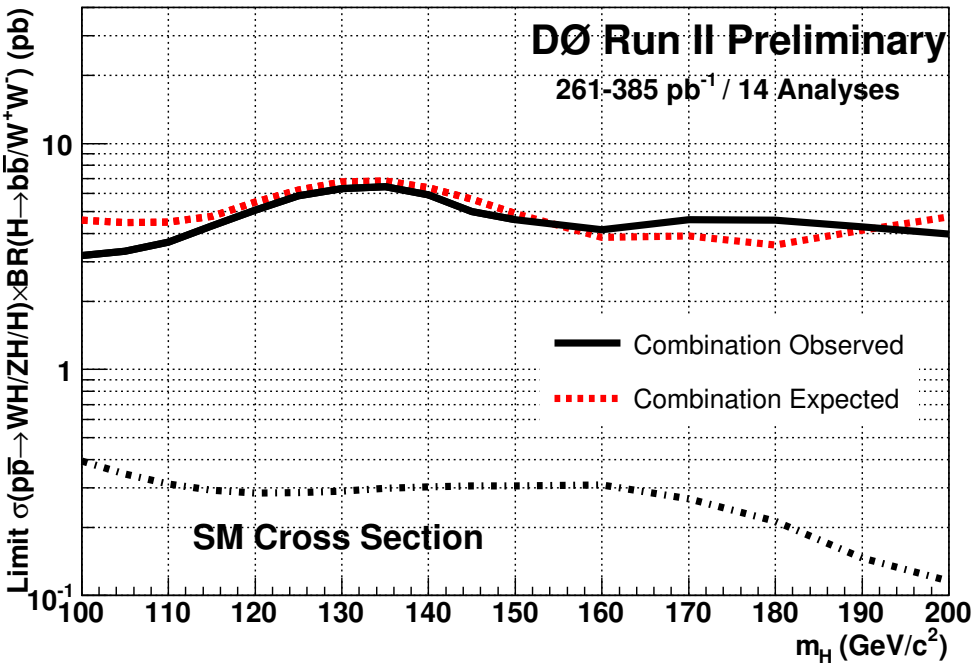

FIG. 9: Expected (median) and observed 95% CL limits for the $WH/ZH/H$ analyses ($WH \to e,\mu,\not\ell\nu b\bar{b}$, $ZH \to \nu\nu b\bar{b}$, $WH \to WW^+W^-$, and $H \to W^+W^-$ final states combined). These limits are given with respect to the sum of $\sigma(p\bar{p} \to WH/ZH) \times BR(H \to b\bar{b})$, $\sigma(p\bar{p} \to WH) \times BR(H \to W^+W^-)$, and $\sigma(p\bar{p} \to H) \times BR(H \to W^+W^-)$ at $\sqrt{s} = 1.96$ TeV. The high-mass range ($m_H = 150 - 200$ GeV/c^2) has contributions only from the $WH \to WW^+W^-$ and $H \to W^+W^-$ analyses.

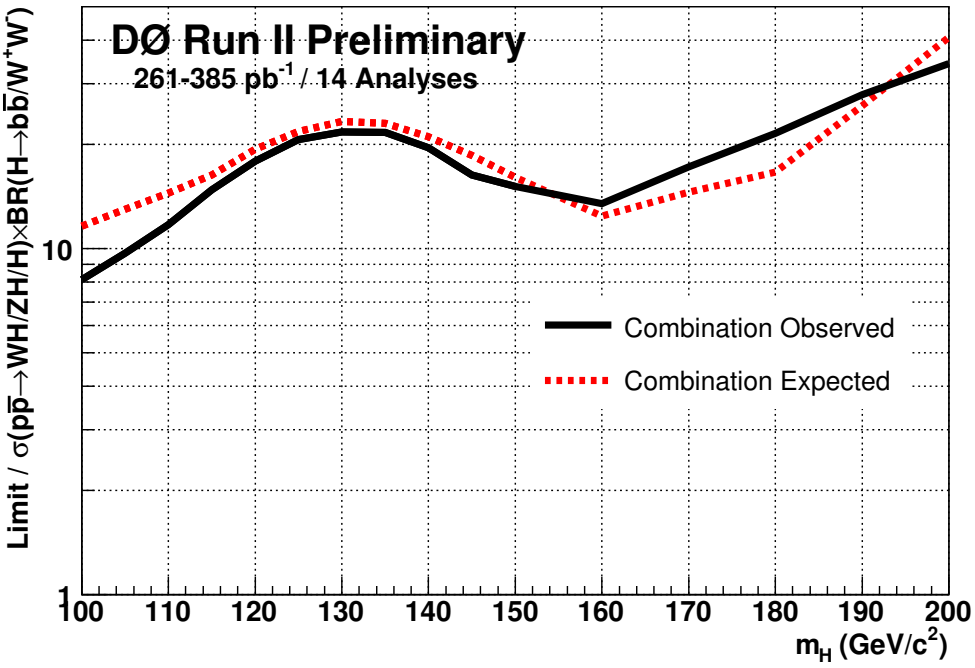

FIG. 10: Expected (median) and observed cross section ratios for the $WH/ZH/H$ analyses ($WH \to e,\mu,\not\ell\nu b\bar{b}$, $ZH \to \nu\nu b\bar{b}$, $WH \to WW^+W^-$, and $H \to W^+W^-$ final states combined). The high-mass range ($m_H = 150-200$ GeV/c^2) has contributions only from the $WH \to WW^+W^-$ and $H \to W^+W^-$ analyses.

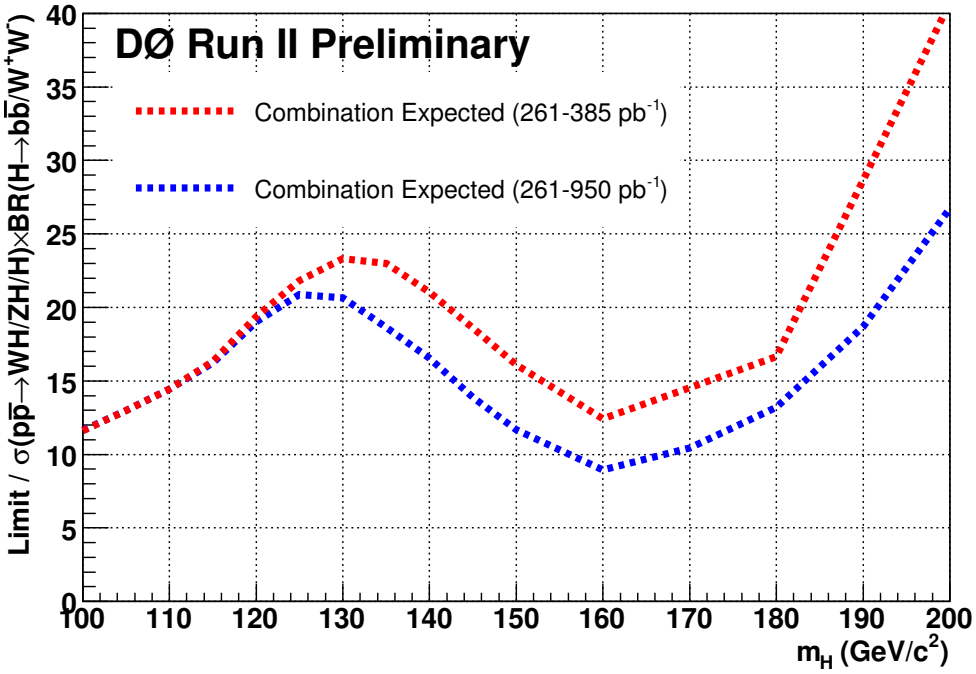

FIG. 11: Expected (median) cross section ratios for the combined limits using two different $H \to W^+W^-$ analyses. The dashed red line uses the lower luminosity channels: $e^{\pm}e^{\mp}$(325 pb^{-1}) and $e^{\pm}\mu^{\mp}$(318 pb^{-1}). The dashed blue line displays the improvement in the expected limit obtained with the higher luminosity channels: $e^{\pm}e^{\mp}$(950 pb^{-1}), $e^{\pm}\mu^{\mp}$(950 pb^{-1}).

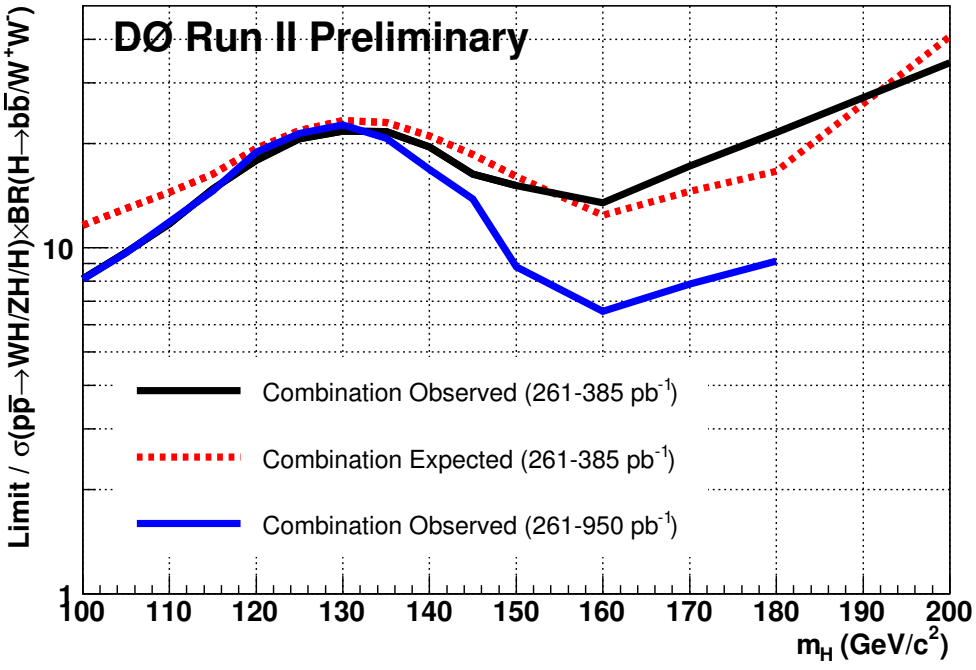

FIG. 12: Comparison of the observed cross section ratios for combined limits using two different $H \to W^+W^-$ analyses. The solid black and blue lines correspond to the observed ratios with the lower luminosity channels ($e^{\pm}e^{\mp}$(325 pb^{-1}) and $e^{\pm}\mu^{\mp}$(318 pb^{-1})) and the higher luminosity channels ($e^{\pm}e^{\mp}$ and $e^{\pm}\mu^{\mp}$(950 pb^{-1})), respectively. The expected combined limit for 261-365 pb^{-1}combination is also shown.